Editors' Suggestion

Direct measurement of the static and transient magneto-optical permittivity of cobalt across the entire *M*-edge in reflection geometry by use of polarization scanning

Dmitriy Zusin,[1,*] Phoebe M. Tengdin,[1] Maithreyi Gopalakrishnan,[1] Christian Gentry,[1] Adam Blonsky,[1] Michael Gerrity,[1] Dominik Legut,[2] Justin M. Shaw,[3] Hans T. Nembach,[3] T. J. Silva,[3] Peter M. Oppeneer,[4] Henry C. Kapteyn,[1] and Margaret M. Murnane[1]

[1]*Department of Physics and JILA, University of Colorado, Boulder, Colorado 80309, USA*
[2]*Nanotechnology & IT4Innovations Center, VSB Technical University Ostrava, CZ-708 33 Ostrava-Poruba, Czech Republic*
[3]*Quantum Electromagnetics Division, National Institute of Standards and Technology, Boulder, Colorado 80305, USA*
[4]*Department of Physics and Astronomy, Uppsala University, S-75120 Uppsala, Sweden*

(Received 13 September 2017; revised manuscript received 15 December 2017; published 30 January 2018)

The microscopic state of a magnetic material is characterized by its resonant magneto-optical response through the off-diagonal dielectric tensor component ϵ_{xy}. However, the measurement of the full complex ϵ_{xy} in the extreme ultraviolet spectral region covering the M absorption edges of 3d ferromagnets is challenging due to the need for either a careful polarization analysis, which is complicated by a lack of efficient polarization analyzers, or scanning the angle of incidence in fine steps. Here, we propose and demonstrate a technique to extract the complex resonant permittivity ϵ_{xy} simply by scanning the polarization angle of linearly polarized high harmonics to measure the magneto-optical asymmetry in reflection geometry. Because this technique is more practical and faster to experimentally implement than previous approaches, we can directly measure the full time evolution of $\epsilon_{xy}(t)$ during laser-induced demagnetization across the entire $M_{2,3}$ absorption edge of cobalt with femtosecond time resolution. We find that for polycrystalline Co films on an insulating substrate, the changes in ϵ_{xy} are uniform throughout the spectrum, to within our experimental precision. This result suggests that, in the regime of strong demagnetization, the ultrafast demagnetization response is primarily dominated by magnon generation. We estimate the contribution of exchange-splitting reduction to the ultrafast demagnetization process to be no more than 25%.

DOI: 10.1103/PhysRevB.97.024433

I. INTRODUCTION

The understanding of strongly coupled interactions in magnetic materials that occur in response to femtosecond laser excitation [1] is critical for advancing our fundamental knowledge of out-of-equilibrium materials systems; however, these are challenging to access both experimentally and theoretically. This knowledge is, moreover, important for utilizing the spin degree of freedom and for designing functional materials [2] and magnetic logic devices that can be controlled by ultrashort light pulses. Such spintronic devices could ultimately be used for fast and energy efficient spin-based logic [3,4]. Because the characteristic spin dynamics of spin-flip processes [5–8], spin transport [9–14], and high-energy spin-wave excitations [15–17] occur on femtosecond to picosecond time scales, their investigation requires ultrashort pulses. To date, most measurements have used either femtosecond visible lasers or short-wavelength synchrotron, free-electron (FEL), and laser-driven x-ray or extreme ultraviolet (EUV) light sources. Ultrafast laser probes have the advantage of very high time resolution and ease of access; however, visible lasers can only measure the net magnetic response of the entire system, with the exception of specific types of systems that contain both rare-earth and transition-metal elements and allow for element specificity in the visible range [18]. Short-wavelength light can, in contrast, access the element-specific magnetic response in alloys and multilayers, without specific requirements for their composition, with the added advantage of broad energy bandwidth that enables measurements across the full M- and L-shell absorption edges that encode a magnetic state.

In previous work, tabletop high harmonic generation (HHG) has been used to explore the competition between spin-flip scattering and spin transport in the ultrafast demagnetization process [13,19]. HHG sources were also recently used to indirectly extract the dynamic permittivity $\epsilon_{xy}(t)$ at two different times—during and after demagnetization and subsequent recovery of the magnetic state—by use of angle-resolved transverse magneto-optical Kerr effect (T-MOKE) measurements, in combination with *ab initio* calculations of the permittivity as a function of exchange splitting and magnon generation [20]. However, the cumbersome need to scan both the time delay and the angle of incidence precluded the direct measurement of the dynamic magneto-optical permittivity $\epsilon_{xy}(t)$ as a continuous function of time, independent of theoretical modeling. Moreover, there are comparable challenges associated with all magneto-optical techniques at EUV and x-ray photon energies. Such challenges include the need for a polarization state analysis in the case of longitudinal MOKE [21–23] and Faraday and Voigt rotation [24–26], scanning the angle of incidence for a measurement of x-ray magnetic circular dichroism (XMCD) in reflection [27], or for a polar MOKE

*dmitriy.zusin@colorado.edu

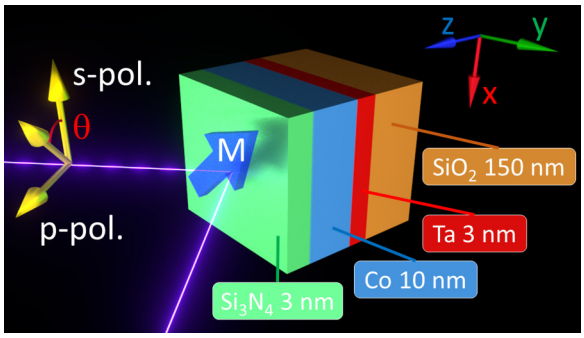

FIG. 1. Schematic of the diagonal magneto-optical effect (D-MOE) and the multilayer sample structure used for the static EUV D-MOE measurements. θ is the angle of the linearly polarized radiation relative to the s-polarization direction.

measurement with an out-of-plane magnetized sample [21,22], or XMCD in transmission geometry [28,29]. As a result, the transient $\epsilon_{xy}(t)$ during ultrafast demagnetization has not yet been measured.

Spin-resolved photoemission spectroscopy can also be used to investigate laser-induced demagnetization dynamics [30–32]. However, photoemission is sensitive only to the top surface of the material. It is also difficult to use for the measurement of the band-structure dynamics across the entire Brillouin zone. In contrast, magneto-optical spectroscopy provides access to the changes of the spin-polarized band structure across the entire Brillouin zone.

In this paper, we present a tabletop EUV magneto-optical technique that can be used to directly measure the complex magneto-optical dielectric tensor element $\epsilon_{xy}(E,t)$ as a function of both photon energy E and time t in order to capture its full dynamic evolution. This technique is therefore complementary to, and in some respects more powerful than, existing approaches. The technique makes use of a diagonal form of the magneto-optical effect, or D-MOE, whereby the magnetization is obliquely oriented to the plane of incidence, as illustrated in Fig. 1. D-MOE can be regarded as a superposition of two magneto-optical geometries, T-MOKE [21,22,33] and the lesser utilized longitudinal magneto-optical effect (L-MOE) [34], which both give rise to a magnetization-dependent reflectivity change. In addition, by scanning the polarization angle of the incident linearly polarized EUV light by rotating the polarization of the driving laser light, we demonstrate that it is possible to uniquely determine $\epsilon_{xy}(E)$, the full complex magneto-optical response. Moreover, the D-MOE geometry naturally lends itself for time-resolved studies for the extraction of $\epsilon_{xy}(E,t)$ as a function of both time and photon energy. By use of the D-MOE geometry for the case of ultrafast demagnetization with a polycrystalline Co film, we find that the fractional variation of $\epsilon_{xy}(E,t)$ over time is effectively independent of E across the entire M-edge to within error bars. This result suggests that the dominant mechanism for ultrafast demagnetization response is magnon generation when the magnetization is quenched by $\sim 42 \pm 5\%$ of its saturation value, i.e., in the regime of strong demagnetization. We estimate an upper limit of 25% for the contribution of the exchange-splitting reduction of the dynamically evolving band structure during ultrafast demagnetization. We note that these findings are consistent within the experimental uncertainty with our previous work [20] that determined the contributions of magnons and exchange-splitting reduction at two specific times during the demagnetization process. Here, however, we access the full dynamic magnetic response as the material first demagnetizes and then begins to recover to its equilibrium state.

To demonstrate the time-resolved capability of D-MOE, we apply this technique to directly measure the static and dynamic $\epsilon_{xy}(E,t)$ at the $M_{2,3}$ absorption edge of 10- and 5-nm polycrystalline Co samples. The time step in our scan is 25 fs, a 28 times improvement over the previous work reported in Ref. [20]. We validate our D-MOE technique using three different approaches: First, we simulate T-MOKE and L-MOE signals on the basis of the dielectric constant values extracted by use of the D-MOE geometry. The simulations compare favorably with experimentally measured T-MOKE and L-MOE data. Second, we confirm that the real and imaginary parts of $\epsilon_{xy}(E)$ satisfy the Kramers-Kronig relations [35]. Finally, we compare our measured ϵ_{xy} with theoretical calculations and also find a very good agreement.

In the following, we derive the D-MOE response at the boundary of two semi-infinite media and show that this effect can be used to uniquely solve for the real and imaginary parts of ϵ_{xy} (see Appendix A). We then generalize this method to multilayer structures and also describe our experimental setup. We also present the static results for a cobalt sample and compare them with theoretical values. Finally, we implement D-MOE on a laser-excited sample. From the dynamic response, we find that there is a uniform reduction of the magnitude of ϵ_{xy} (cf. Ref. [20]), within our error bars, suggesting that, for strong quenching, the demagnetization response is dominated primarily by ultrafast magnon generation with a possible smaller contribution from the dynamically evolving band structure (i.e., exchange-splitting reduction).

II. EXPERIMENTAL SETUP

The experimental setup is shown in Fig. 2. Near-infrared (NIR) pulses at 790 nm with an energy of 1.2 mJ and at a 5 kHz repetition rate from an amplified ultrafast laser (KMLabs Wyvern) are focused into a hollow waveguide filled with He gas, where the EUV light is generated by the HHG process. We then direct the EUV probe beam onto the sample by use of a toroidal mirror, which focuses the probe beam onto an x-ray CCD camera after it impinges on a diffraction grating for spectral resolution. The sample itself is placed in front of a projection-field electromagnet that applies a magnetic field to the sample. The electromagnet can be rotated to magnetize the sample in the D-MOE geometry, which is at an angle to the plane of incidence of the EUV probe. The resultant reflectometry spectra measured in this geometry at different polarization angles of the linearly polarized probe are amenable to the unique determination of the magneto-optical dielectric constant—without any model-dependent constraints. Details on the mathematical analysis that proves this result can be found in Appendix A. To extract the spectrally resolved D-MOE, the reflected HHG beam is dispersed by a diffraction grating that is mounted in a conical configuration for higher efficiency [36]. Aluminum foil filters of submicron thicknesses

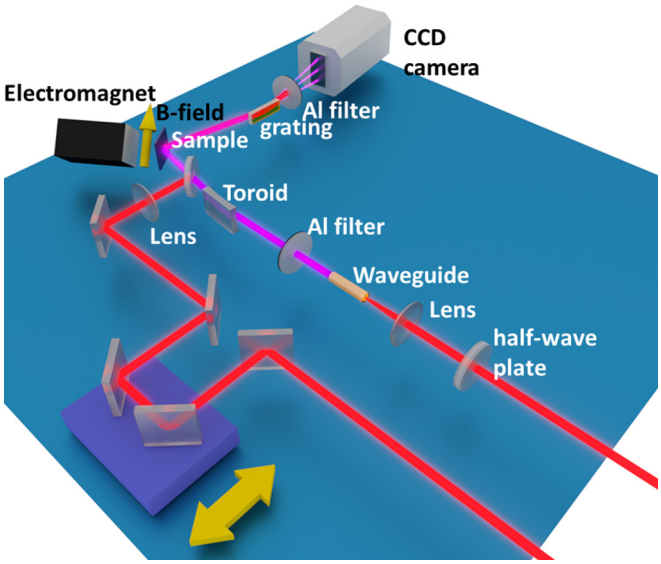

FIG. 2. Experimental setup to implement D-MOE. A half-wave plate is used to rotate the linear polarization of the driving laser, and hence the polarization of the HHG beam.

are used to reject any residual NIR light. For investigating laser-driven ultrafast demagnetization, we direct a fraction of the NIR light into a pump beam with a fluence of 2.7 mJ/cm^2 and p polarization at the sample. The pump beam is collinear with the probe beam. Because the NIR light is generated by the same Ti:sapphire laser, the laser pump pulses are intrinsically synchronized with the EUV probe pulses, with virtually no jitter. The polarization direction of the generated EUV light is identical to that of the driving laser due to the nature of the HHG process [37,38]. As such, the polarization of the EUV probe is controlled by use of a half-wave plate to rotate the linear polarization angle of the driving laser beam.

III. RESULTS AND DISCUSSION

By use of the D-MOE geometry and a continuously rotated linear polarization of the probe beam, we extracted the off-diagonal component of the dielectric tensor for two multilayer samples. The first sample, also shown in Fig. 1, is a multilayer stack consisting of $Si/SiO_2(150)/Ta(3)/Co(10)/Si_3N_4(3)$, where all thicknesses are reported in nanometers. Static polarization scans on the Co multilayer stack were done at three different orientations of the magnetization vector $\vec{m}$: transverse, longitudinal, and diagonal at 45° to the plane of incidence of the EUV probe. Extraction of the ϵ_{xy} over the full energy range of the Co M-edge follows the method described in Appendix A, and the diagonal components of the dielectric constant used in the extraction of the ϵ_{xy} were taken from Ref. [39]. The experimental data for the three geometries, as well as the simulated magneto-optical signals based on the ϵ_{xy} extracted from D-MOE, are shown in Fig. 3. The experimental points on the energy axis in Fig. 3 correspond to the harmonic peaks of the HHG probe spectrum. We can accurately calculate the magneto-optical reflectivity for both the T-MOKE and L-MOE geometries by use of the ϵ_{xy} extracted from the spectroscopic reflectivity data in the D-MOE geometry, as evidenced by the excellent agreement between the experimental and simulated data in Figs. 3(b) and 3(e), as well as Figs. 3(c) and 3(f). Conversely, we show in Fig. 4 that it is not possible to extract the correct general ϵ_{xy} from either the longitudinal or the transverse geometries by simply scanning the polarization, as discussed in Appendix A. This is because, in order to extract the full ϵ_{xy}, they require

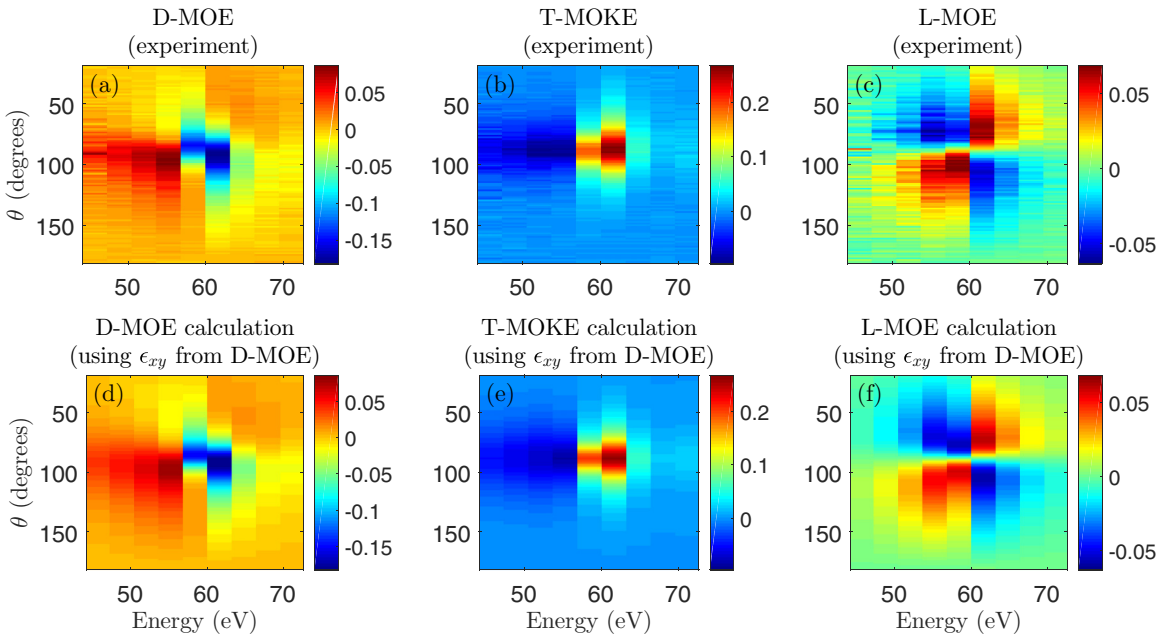

FIG. 3. Energy- and polarization angle-dependent magneto-optical spectra for the three orientations of the magnetization $\vec{m}$: (a) D-MOE, (b) T-MOKE, and (c) L-MOE. The data are measured at the discrete harmonic peaks of the EUV probe spectrum. Polarization angle $\theta = 90°$ corresponds to p polarization. (d)–(f) are calculations for each geometry generated from the ϵ_{xy} that is extracted from fitted measurements in the D-MOE geometry.

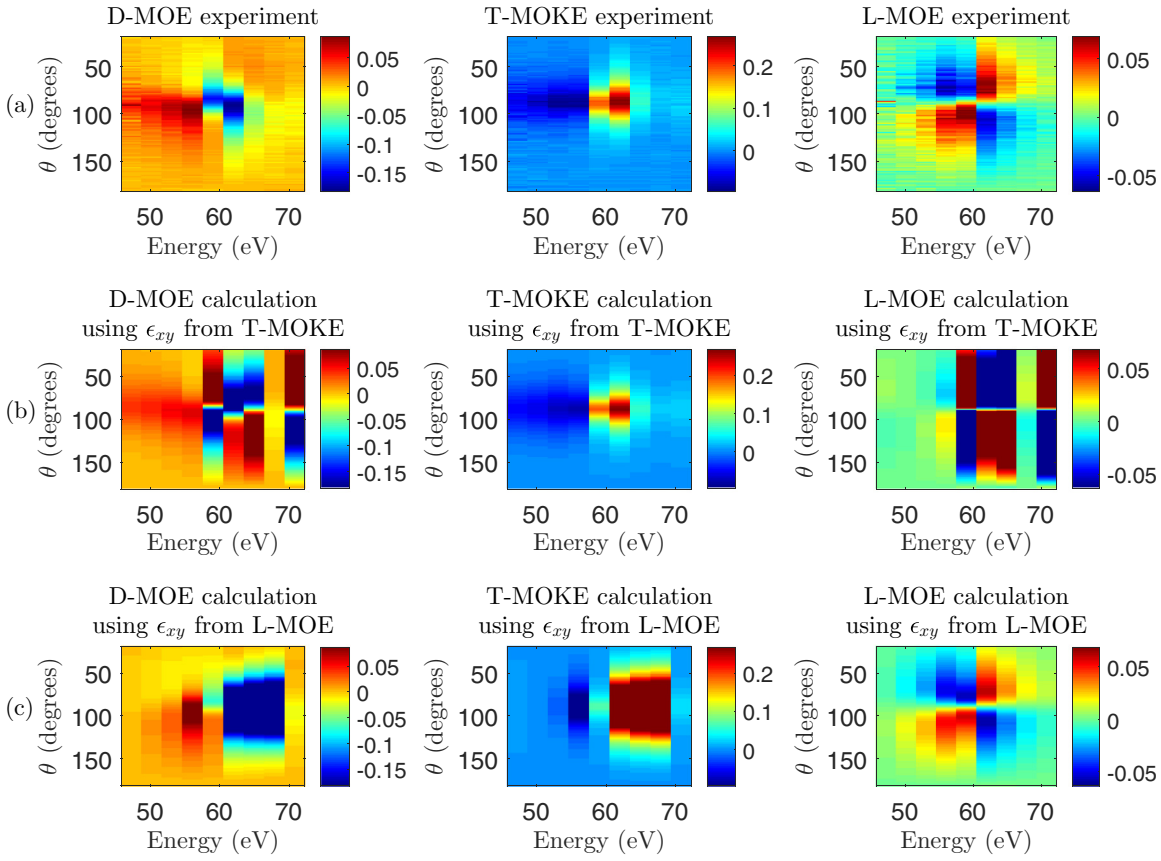

FIG. 4. (a) Polarization-resolved EUV magneto-optical signals with their reconstructions made using ϵ_{xy} extracted from (b) T-MOKE and (c) L-MOE. Note that the ϵ_{xy} extracted from the T-MOKE and L-MOE spectra are only capable of providing satisfactory reconstructions of their own signal, and not capable of reconstructing the signals in other geometries without scanning the angle of incidence. The same set of polarization angles was used for all the geometries shown in the figure.

additional information, e.g., by scanning the angle of incidence in fine steps. Such an approach is possible, but very challenging for time-resolved measurements.

An additional test of the fitted results is to verify if the real and imaginary parts of the extracted ϵ_{xy} are consistent with the Kramers-Kronig relations. As can be seen from Fig. 5, the real part of ϵ_{xy} obtained by applying a Kramers-Kronig transform to the interpolant of the imaginary part is consistent with the experimental values to within the measurement precision. The self-consistency of the measured ϵ_{xy} with the Kramers-Kronig relations is evidence in support of the D-MOE method. Furthermore, the extracted ϵ_{xy} spectra compare favorably with theoretical calculations (from Ref. [20]), which are also shown in Fig. 5.

Having validated our D-MOE technique, we employed it in a stroboscopic pump-probe experiment to extract the dynamic evolution of $\epsilon_{xy}(E,t)$ on femtosecond time. For this purpose, we used the second sample, a 5-nm-thick Co film grown on an insulating substrate without the presence of the seed layer, in order to isolate the dynamic changes in ϵ_{xy} as solely the result of local microscopic processes, as opposed to the generation of laser-induced spin currents [9,13] which are nonlocal. We note that such extraction of the dynamic $\epsilon_{xy}(E,t)$ is only valid in the quasistatic approximation when changes in ϵ_{xy} are much slower compared to, in particular, the duration of the probe pulses. This is indeed the case since the characteristic time constant of ∼230 fs for a dynamically evolving ϵ_{xy} is much longer than the duration of the sub-10-fs EUV probe pulses. Additionally, we constrain our analysis to time scales exceeding 100 fs—where we do not overlap with the 50-fs

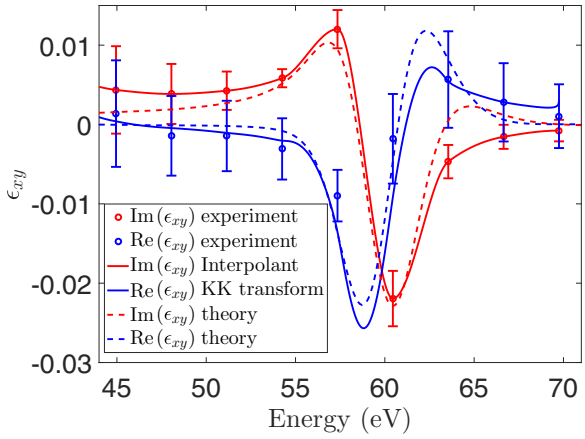

FIG. 5. Experimental ϵ_{xy} measured at the M-edge of Co, on a Si/SiO_2(150)/Co(5)/GeO_2(3) multilayer. Our data compare well with theoretical calculations [20], and the real and imaginary parts satisfy the Kramers-Kronig relations. The error bars are estimated based on the root-mean-square deviation of the HHG intensity (see Appendix C) for details.

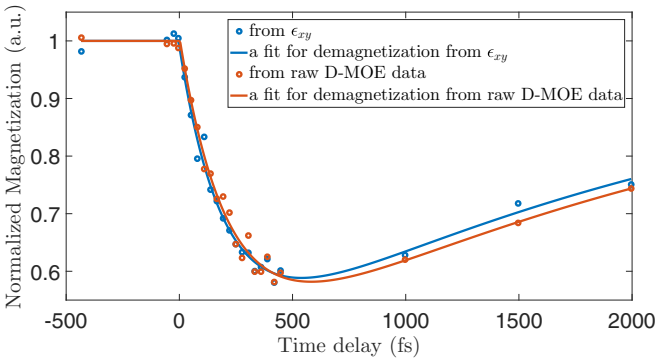

FIG. 6. Normalized laser-induced demagnetization response of a $Si/SiO_2(150)/Co(5)/GeO_2(3)$ multilayer.

near-infrared pump pulse, and dynamic changes in ϵ_{xy} are large enough for us to draw definitive conclusions from the data given our experimental uncertainty.

We measured the dynamic magneto-optical response over a range of polarization angles from 30° to 150° with respect to s polarization, as shown in Fig. 1. We used angle steps of 6.7° and time steps of 25 fs. The observed demagnetization response is shown in Fig. 6. It exhibits a fast reduction in magnetization, with an exponential time constant of ∼233 fs, followed by a slower exponential recovery of ∼2.4 ps. In the figure, two signals are compared: based on the raw data and that calculated from the dynamics of $\epsilon_{xy}(E,t)$. The raw data response (red circles) was obtained by averaging the signal over multiple discrete harmonic peaks and all measured polarization angles. To improve the signal-to-noise ratio, integration was limited to angles and energies where the absolute value of the magneto-optical asymmetry exceeds 0.12 before time zero. The response based on the dynamics of $\epsilon_{xy}(E,t)$ (blue circles) was calculated from the integrated response of $\mathrm{Im}(\epsilon_{xy})$ over the energy range of 55–63 eV. The two methods agree well: The decay τ_D and recovery τ_R time constants of the standard double-exponential fit [40] are $\tau_D = 224 \pm 53$ fs and $\tau_R = 2302 \pm 623$ fs, based on the dynamics of $\epsilon_{xy}(E,t)$, and $\tau_D = 242 \pm 58$ fs and $\tau_R = 2417 \pm 686$ fs, based on the raw D-MOE data.

From the polarization-resolved data, we extracted ϵ_{xy} at each time step in Fig. 6. The resulting evolution of the differential change $\Delta\epsilon_{xy}(E,t) = \epsilon_{xy}(E,t) - \epsilon_{xy}(E,t<0)$ is shown in Figs. 7(a) and 7(b) for both the real and imaginary parts, respectively. The data clearly show a transient decrease and recovery of ϵ_{xy} after laser excitation. The fundamental mechanisms underlying ultrafast laser-induced demagnetization have been intensely debated ever since the effect was first observed [5,8,20,32,41–46]. Since nonlocal spin transport is minimized with the here-chosen sample geometry [9], the remaining possible mechanisms are longitudinal spin flips, e.g., caused by electron-phonon scattering, that would eventually lead to a reduction of the exchange splitting [5,7,47], or demagnetization due to ultrafast nonequilibrium magnon generation [8,15,17]. The former mechanism reduces the magnitude of the magnetization vector, while the latter preserves its magnitude but tilts the magnetization locally. Both types of excitation result in a reduced projection of the magnetization on a local z axis, which can be measured by use of magneto-optical techniques. These mechanisms map onto the basic models of ferromagnetism in metallic systems: the Stoner picture [48], and the Heisenberg picture [49,50]. As proposed

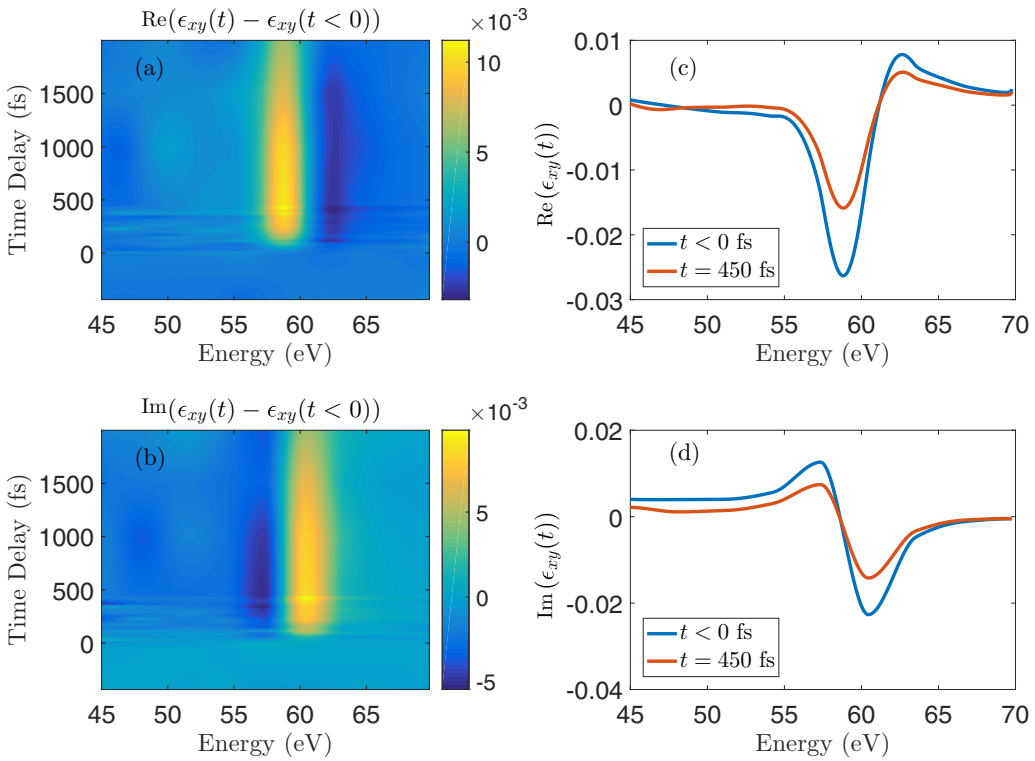

FIG. 7. Time-resolved differential changes in the (a) real and (b) imaginary parts of ϵ_{xy} with respect to the ground state at $t < 0$ fs and (c) real and (d) imaginary parts of ϵ_{xy} at $t < 0$ fs and $t = 450$ fs.

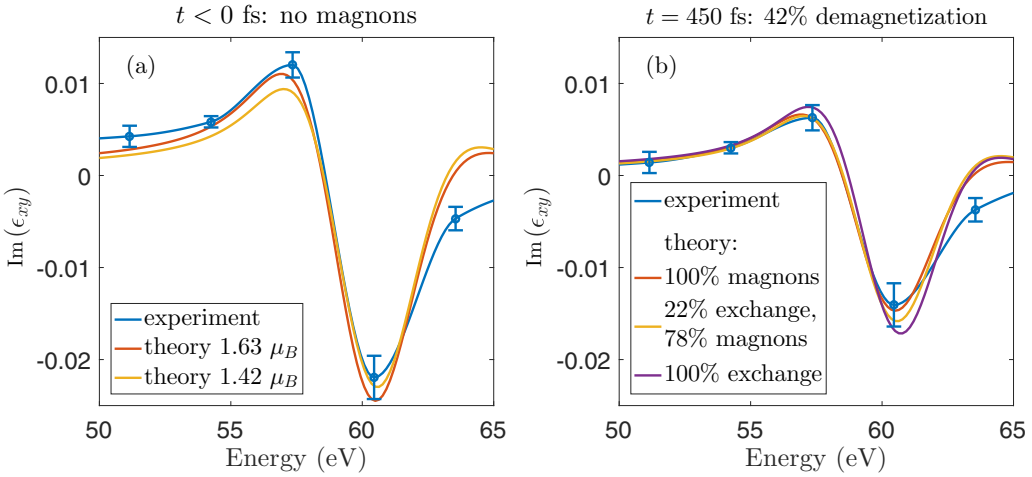

FIG. 8. Comparison of the experimental ϵ_{xy} with the theoretical values calculated *ab initio* for the ground state as well as excited states of cobalt with reduced values of exchange splitting. (a) $t \leqslant 0$ fs, where theory does not include any magnon excitation. (b) $t = 450$ fs, where the theory curves have been scaled as if demagnetization was entirely due to magnon generation (red curve), and also when $\sim 3/4$ and $\sim 1/4$ of the total 42% demagnetization were due to magnons and exchange-splitting reduction, respectively (yellow curve), and when the demagnetization was entirely due to exchange-splitting reduction (purple curve). Since the difference between the theoretical ϵ_{xy} for the cases of 78% and 100% magnon contribution (yellow and red curves) to the total demagnetization lies within the experimental error bars (see Appendix C), while it is outside of the error bars for the case of 100% exchange reduction contribution (purple curve), we conclude that exchange-splitting reduction plays a lesser role in the magnetization reduction, contributing at most $\sim 1/4$ of the observed signal.

in 1975 by Erskine and Stern when they first predicted x-ray magnetic circular dichroism (XMCD) [51], these two theories of ferromagnetism each lead to specific spectral changes in ϵ_{xy} through which one could distinguish which mechanism was operative. The predicted effect of these two mechanisms on the time-resolved magneto-optical spectrum was confirmed recently by *ab initio* calculations; transverse spin excitations lead to a spectrally uniform, linear decrease of the amplitude of ϵ_{xy} [20]. Reducing or enhancing the Stoner exchange splitting, on the other hand, has been shown to lead to changes of peak positions in addition to nonlinear changes in MOKE peak amplitudes [20,52].

As shown in Fig. 8, to within the error bars of our measurement, the change in ϵ_{xy} after laser excitation appears uniform across the entire M-edge between 45 and 70 eV. This is consistent with the predicted behavior for ultrafast magnon generation. However, a nonzero reduction of the exchange splitting cannot be excluded, given the measurement precision. To illustrate this, in Fig. 8(b) we plot three theoretically calculated Im(ϵ_{xy}) curves—one with an unperturbed exchange splitting and two with a quenched exchange leading to a reduction of the magnitude of the magnetic moment from $1.63\mu_B$ to $1.42\mu_B$ and to $0.97\mu_B$—along with the measured Im(ϵ_{xy}) at 450 fs. Notably, the theoretical curves also take into account the respective magnon contributions such that the net demagnetization of all three curves is at the experimentally measured value of 42%, i.e., the projection of the magnetic moment on the local z axis is reduced from $1.63\mu_B$ to $0.97\mu_B$, for the three cases. The demagnetization is either entirely due to magnons [red curve in Fig. 8(b)] or to exchange-splitting reduction [purple curve in Fig. 8(b)], or magnons contribute $\sim 3/4$ to the signal, while exchange reduction contributes $\sim 1/4$ of the signal [yellow curve in Fig. 8(b)]. As can be seen from the figure, the theoretical ϵ_{xy} have different spectral shapes, which confirms the prediction made by Erskine and Stern [51]. For details on the theoretical ϵ_{xy} for various values of exchange splitting, see Appendix D. An ϵ_{xy} that results solely from a reduced exchange splitting does not fit the experimental data well, and thus we exclude the collapse of exchange splitting as the single driver of ultrafast demagnetization. The biggest change occurs around 60.5 eV. However, for the yellow curve in Fig. 8(b), this change is still within the experimental error. This puts an upper limit on the possible contribution of the exchange-splitting reduction to the net demagnetization: To within the estimated measurement precision for the magnitude of ϵ_{xy} of $\sim 25\%$ at 60.5 eV, the upper limit for the relative contribution of exchange-splitting reduction is also $\sim 25\%$. Conversely, no less than $\sim 75\%$ of the laser-induced demagnetization is dominated by ultrafast magnon generation. This result is consistent with both our previous work [20], and with recent transient spin-resolved photoemission measurements [32].

We would like to note that, because of the inherent experimental uncertainty, our D-MOE technique yields useful information when transient changes in ϵ_{xy} are sufficiently large. On sub-100-fs time scales, such changes are subtle, and further work is needed to determine the microscopic mechanisms at work on such fast times. It has been proposed that the spin-orbit interaction [53,54] plays an important role in the initial demagnetization that takes place in the spin-polarized valence states. The spin-orbit interaction in the valence band, which is much smaller than that in the semicore states, can lead through electron-phonon scattering to longitudinal spin flips that cause a reduction of the exchange splitting [5].

IV. SUMMARY

We found that for a Co multilayer grown on an insulating substrate, the changes in ϵ_{xy} caused by ultrafast demagnetization were uniform across the M-edge, within the experimental uncertainty. This finding suggests that laser-

induced demagnetization, in the limit of strong quenching, predominantly results from ultrafast nonequilibrium magnon generation with a possible, yet quite smaller, contribution from a dynamically reduced exchange splitting. Our measurements thus provide a strong support of ultrafast magnon generation [8] as a dominant mechanism of laser-induced demagnetization on subpicosecond time scales, in contrast to a quenching of the exchange splitting [5,7] caused by fast spin-flip scattering. Further work is needed to determine the cause of the ultrafast magnon generation on sub-100-fs time scales, and longitudinal spin flips and the spin-orbit interaction [53,54] seem to be promising candidates for that role. To obtain the spectra utilized in this study, we demonstrated a method for efficient extraction of the off-diagonal dielectric tensor component across the M-shell absorption edge of a magnetic material in a reflection geometry by measuring the magneto-optical response of a multilayer sample at different polarization angles of the probe beam from a laser-driven tabletop HHG source. This method is very well suited for measuring the full transient magneto-optical response to an intense near-infrared laser pulse with femtosecond time resolution. In the future, we expect that D-MOE measurements can be combined with density functional theory (DFT) calculations to map the full dynamic band structure of a demagnetizing magnetic material.

ACKNOWLEDGMENTS

This work was done at JILA; H.C.K. and M.M.M. acknowledge support from the Department of Energy (DOE) Office of Basic Energy Sciences X-Ray Scattering Program Award No. DE-SC0002002 and a Gordon and Betty Moore Foundation EPiQS Award through Grant No. GBMF4538. P.M.O. acknowledges financial support from the Swedish Research Council (VR) and the Knut and Alice Wallenberg Foundation (Grant No. 2015.0060). D.L. acknowledges support by the European Regional Development Fund in the IT4Innovations national supercomputing center Path to Exascale project, No. CZ.02.1.01/0.0/0.0/16_013/0001791 within the Operational Programme Research, Development and Education and Grant No. 17-27790S of the Czech Science Foundation. The authors acknowledge fruitful discussions with Karel Carva, Emrah Turgut, and Patrik Grychtol.

Contributions to this article by workers at NIST, an agency of the U.S. Government, are not subject to U.S. copyright. H.C.K. and M.M.M. have a financial interest in KMLabs. Any identification of commercial equipment, instruments, or materials is not intended as an endorsement by NIST.

APPENDIX A: TWO-AXIS MAGNETO-OPTICAL EFFECT D-MOE

We first consider D-MOE at an interface as shown in Fig. 1. In the s- and p-polarization basis (E_s, E_p), the incident electric field $\vec{E}_i$, i.e., the time- and space-independent part of the plane-wave radiation, can be written as

$$\vec{E}_i = \begin{pmatrix} E_s \\ E_p \end{pmatrix} = \begin{pmatrix} \cos\theta \\ \sin\theta \end{pmatrix} E_0, \tag{A1}$$

where E_0 is the amplitude of the incoming electric field vector; in the following, we shall set E_0 to 1. θ is the angle of the linearly polarized radiation relative to the s-polarization direction. The reflected field $\vec{E}_r$ is related to the incident field through the 2×2 bulk Fresnel reflection matrix $\hat{\mathbf{r}}$ as

$$\vec{E}_r = \hat{\mathbf{r}}\vec{E}_i = \hat{\mathbf{r}}\begin{pmatrix} \cos\theta \\ \sin\theta \end{pmatrix}. \tag{A2}$$

This matrix depends on the magnetization direction $\vec{m}$ (see, e.g. Refs. [35,55]); when $\vec{m}$ lies in the (x,y) plane, i.e., $\vec{m} = (m_x, m_y, 0)$, as in Fig. 1, it can be expressed to first order in the magneto-optical Voigt constant $Q = i\epsilon_{xy}/\epsilon_{xx}$ as

$$\hat{\mathbf{r}}(\vec{m}) = \begin{pmatrix} r_{ss} & r_{sp} \\ r_{ps} & r_{pp} \end{pmatrix} \simeq \begin{pmatrix} r_{ss}^{(0)} & r_{sp}^{(1)} m_y Q \\ -r_{sp}^{(1)} m_y Q & r_{pp}^{(0)} + r_{pp}^{(1)} m_x Q \end{pmatrix}, \tag{A3}$$

where the superscripts (0) and (1) indicate the coefficients in terms independent of and linear in Q, respectively. Note that $r_{ss}^{(0)} \equiv r_{ss}$. To quantify the difference in reflectivity from the boundary for two opposite directions of $\vec{m}$, we define a quantity called the magneto-optical asymmetry A as the normalized reflectivity difference,

$$A = \frac{R_+ - R_-}{R_+ + R_-}, \tag{A4}$$

where $R_\pm = |\vec{E}_r(\pm\vec{m})|^2$. From Eqs. (A2)–(A4), one can show that the asymmetry for a sample magnetized in plane, with components along the x and y axes, to a first order in Q, is

$$A = \frac{m_y \sin 2\theta \,\mathrm{Re}\left[\left(r_{ss} - r_{pp}^{(0)}\right)^* r_{sp}^{(1)} Q\right] - m_x\left(1 - \cos 2\theta\right)\mathrm{Re}\left(r_{pp}^{(0)*} r_{pp}^{(1)} Q\right)}{\left|r_{pp}^{(0)}\right|^2 \sin^2\theta + |r_{ss}|^2 \cos^2\theta}, \tag{A5}$$

where Re is the real part of an expression.

We now consider special cases of expression (A5) for the transverse $\vec{m} = (1,0,0)$, longitudinal $\vec{m} = (0,1,0)$, and mixed $\vec{m} = \frac{1}{\sqrt{2}}(1,1,0)$ magnetization directions. For the transverse configuration, we obtain

$$A_T := A(m_x = -1; m_y = 0) = \frac{(1 - \cos 2\theta)\mathrm{Re}\left(r_{pp}^{(0)*} r_{pp}^{(1)} Q\right)}{\left|r_{pp}^{(0)}\right|^2 \sin^2\theta + |r_{ss}|^2 \cos^2\theta}, \tag{A6}$$

which matches with the well-known T-MOKE asymmetry [56] which is normally defined for p-polarized light, i.e., for $\theta = \pi/2$. We also recover the result for the L-MOE in the longitudinal configuration [34],

$$A_L := A(m_x = 0; m_y = 1) = \frac{\sin 2\theta \,\mathrm{Re}\left[\left(r_{ss} - r_{pp}^{(0)}\right)^* r_{sp}^{(1)} Q\right]}{\left|r_{pp}^{(0)}\right|^2 \sin^2\theta + |r_{ss}|^2 \cos^2\theta}. \tag{A7}$$

For L-MOE, note that the reflectivity change is zero for the case of s- or p-polarized light, i.e., $\theta = 0,\pi/2$, and thus an incident beam with a mixed polarization state is needed to observe a magnetization-dependent reflectivity change.

Next, we show that it is possible to obtain a unique solution for the complex Q in the D-MOE geometry, while also demonstrating that it is impossible to use longitudinal or transverse geometries for this purpose. We choose a symmetric configuration with the magnetization set at 45° with respect to the scattering plane, i.e., $\vec{m} = \frac{1}{\sqrt{2}}(1,1,0)$. We would like to emphasize that the results would still hold for any other configuration as well, as long as both m_x and m_y magnetization components are nonzero. For our case, after expanding the real part in (A5) as $\mathrm{Re}(z) = \frac{1}{2}(z + z^*)$, the magneto-optical asymmetry reads

$$A_D := A\left(m_x = -\frac{1}{\sqrt{2}}; m_y = \frac{1}{\sqrt{2}}\right) = F_D(\theta)Q + F_D^*(\theta)Q^*, \tag{A8}$$

where we defined the complex factor $F_D(\theta)$ as

$$F_D(\theta) = \frac{\sin 2\theta\left(r_{ss} - r_{pp}^{(0)}\right)^* r_{sp}^{(1)} + (1 - \cos 2\theta) r_{pp}^{(0)*} r_{pp}^{(1)}}{2\sqrt{2}\left(\left|r_{pp}^{(0)}\right|^2 \sin^2\theta + |r_{ss}|^2 \cos^2\theta\right)}. \tag{A9}$$

To exemplify how this is different from A_T and A_L, we rewrite A_T and A_L in a similar form,

$$A_T = F_T(\theta)Q + F_T^*(\theta)Q^* \equiv f_T(\theta)\left(r_{pp}^{(0)*} r_{pp}^{(1)} Q + r_{pp}^{(0)} r_{pp}^{(1)*} Q^*\right), \tag{A10}$$

$$A_L = F_L(\theta)Q + F_L^*(\theta)Q^* \equiv f_L(\theta)\left[\left(r_{ss} - r_{pp}^{(0)}\right)^* r_{sp}^{(1)} Q + \left(r_{ss} - r_{pp}^{(0)}\right) r_{sp}^{(1)*} Q^*\right], \tag{A11}$$

with $f_T(\theta)$ and $f_L(\theta)$ [as well as $F_T(\theta)$ and $F_L(\theta)$] defined as

$$f_T(\theta) \equiv \frac{F_T(\theta)}{r_{pp}^{(0)*} r_{pp}^{(1)}} = \frac{(1 - \cos 2\theta)}{2\left(\left|r_{pp}^{(0)}\right|^2 \sin^2\theta + |r_{ss}|^2 \cos^2\theta\right)}, \tag{A12}$$

$$f_L(\theta) \equiv \frac{F_L(\theta)}{\left(r_{ss} - r_{pp}^{(0)}\right)^* r_{sp}^{(1)}} = \frac{\sin 2\theta}{2\left(\left|r_{pp}^{(0)}\right|^2 \sin^2\theta + |r_{ss}|^2 \cos^2\theta\right)}. \tag{A13}$$

It is important to note that the prefactors $f_T(\theta)$ and $f_L(\theta)$, which contain the angular dependence, are purely real, while $F_D(\theta)$ has a complex dependence on θ. In order to solve for Q and Q^* and thus find the real and imaginary parts of Q, we need two linearly independent equations. We can obtain those by measuring the magneto-optical asymmetry at two different polarization angles θ_1 and θ_2. This leads to a system of equations that can be written in a matrix form as

$$\begin{pmatrix} a_x & b_x \\ c_x & d_x \end{pmatrix}\begin{pmatrix} Q \\ Q^* \end{pmatrix} = \begin{pmatrix} A_x(\theta_1) \\ A_x(\theta_2) \end{pmatrix}, \tag{A14}$$

where the subscript $x = T$, L, or D. We write explicitly the system matrix $\Lambda_{\mathbf{x}}$ for the transverse, longitudinal, and diagonal cases using Eqs. (A11), (A12), and (A9), respectively,

$$\Lambda_{\mathbf{T}} := \begin{pmatrix} a_T & b_T \\ c_T & d_T \end{pmatrix} = \begin{pmatrix} f_T(\theta_1) r_{pp}^{(0)*} r_{pp}^{(1)} & f_T(\theta_1) r_{pp}^{(0)} r_{pp}^{(1)*} \\ f_T(\theta_2) r_{pp}^{(0)*} r_{pp}^{(1)} & f_T(\theta_2) r_{pp}^{(0)} r_{pp}^{(1)*} \end{pmatrix}, \tag{A15}$$

$$\Lambda_{\mathbf{L}} := \begin{pmatrix} a_L & b_L \\ c_L & d_L \end{pmatrix} = \begin{pmatrix} f_L(\theta_1)\left(r_{ss} - r_{pp}^{(0)}\right)^* r_{sp}^{(1)} & f_L(\theta_1)\left(r_{ss} - r_{pp}^{(0)}\right) r_{sp}^{(1)*} \\ f_L(\theta_2)\left(r_{ss} - r_{pp}^{(0)}\right)^* r_{sp}^{(1)} & f_L(\theta_2)\left(r_{ss} - r_{pp}^{(0)}\right) r_{sp}^{(1)*} \end{pmatrix}, \tag{A16}$$

$$\Lambda_{\mathbf{D}} := \begin{pmatrix} a_D & b_D \\ c_D & d_D \end{pmatrix} = \begin{pmatrix} F_D(\theta_1) & F_D^*(\theta_1) \\ F_D(\theta_2) & F_D^*(\theta_2) \end{pmatrix}. \tag{A17}$$

In order for a linear system with a nonzero right-hand side to have a unique solution, the determinant of the system matrix must be nonzero. For the matrices (A15)–(A17), the determinants are

$$\det \Lambda_{\mathbf{T}} = f_T(\theta_1) f_T(\theta_2)\left(\left|r_{pp}^{(0)}\right|^2 \left|r_{pp}^{(1)}\right|^2 - \left|r_{pp}^{(0)}\right|^2 \left|r_{pp}^{(1)}\right|^2\right) \equiv 0, \tag{A18}$$

$$\det \Lambda_{\mathbf{L}} = f_L(\theta_1) f_L(\theta_2)\left(\left|r_{ss} - r_{pp}^{(0)}\right|^2 \left|r_{sp}^{(1)}\right|^2 - \left|r_{ss} - r_{pp}^{(0)}\right|^2 \left|r_{sp}^{(1)}\right|^2\right) \equiv 0, \tag{A19}$$

$$\det \Lambda_{\mathbf{D}} = F_D(\theta_1) F_D^*(\theta_2) - F_D^*(\theta_1) F_D(\theta_2) \neq 0. \tag{A20}$$

The determinants for the transverse and longitudinal magnetization geometries vanish, while the nonzero determinant is possible only in the diagonal two-axis geometry under the condition that $\cos(\theta_1)\sin(\theta_2) \neq \sin(\theta_1)\cos(\theta_2)$, which is fulfilled when $\theta_{1,2} \neq 0$ and $\theta_1 \neq \theta_2$. The latter geometry can thus be used to extract the full complex Q, and hence ϵ_{xy}, by measuring the D-MOE response at different polarization angles.

For the case of thin-film samples with a multilayer structure, such as in Fig. 1, interference effects must be taken into account in order to accurately extract ϵ_{xy}. To do this, we compute the magneto-optical reflectivity of the sample for opposite

directions of $\vec{m}$ by use of the multilayer modeling formalism of Zak *et al.* [57]. From the computed reflectivity, we then calculate the D-MOE asymmetry to compare with the data. Because this method does not utilize an analytic expression, extraction starts with a guess solution for ϵ_{xy} that is then iteratively adjusted until the calculated polarization angle-dependent magneto-optical asymmetry fits the experimentally measured signal to within the experimental uncertainties. As we show in Sec. III, the multilayer fitting procedure is robust for the particular sample considered.

APPENDIX B: EFFECT OF OPTICAL ELEMENTS ON THE MAGNETO-OPTICAL SIGNAL

Here, we verify that the toroidal mirror and the diffraction grating do not affect our measurements. The former could potentially introduce ellipticity into the probe beam, while the latter could have varying diffraction efficiencies for different polarization directions which could distort the measured magneto-optical response of the sample. While the reflectance of the mirror does depend on the polarization of the incident light, it does not affect our measurements since we are interested in the relative change of the magneto-optical reflectivity upon a full reversal of the sample's magnetization and not in its absolute magnitude. For a toroidal mirror consisting of a Pyrex glass substrate coated with 100 nm of B_4C, we calculate for the S_3 Stokes parameter of the reflected beam normalized by the total intensity, a value $S_3 \leqslant 0.11$ ($S_3 = 0$ for linear and $S_3 = \pm 1$ for circular polarization) at a 6° grazing incidence. This means that the electric field on the minor semiaxis of the polarization ellipse is less than 0.055 of the field on the major semiaxis. Such a small ellipticity can be neglected for our purposes.

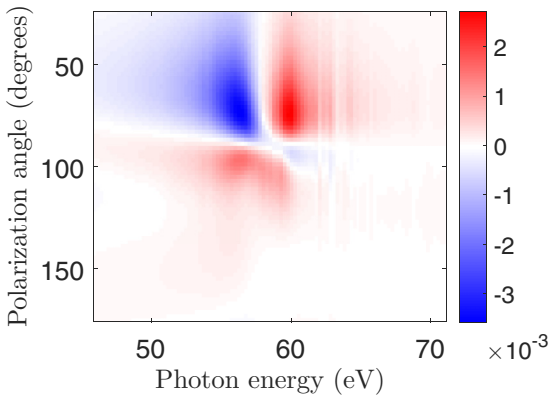

FIG. 9. Influence of the spectrometer diffraction grating on the measured D-MOE asymmetry: Difference in diffraction efficiencies of the light reflected from a cobalt multilayer $Si/SiO_2(150)/Ta(3)/Co(10)/Si_3N_4(3)$ for the two opposite magnetization directions $\pm\vec{m}$. A sawtooth grating made of Zerodur glass and coated with 30 nm of B_4C with a period of 2 μm and a blaze angle of 4.7° was set in a conical configuration at a 5° grazing incidence, and the grating vector was turned by 2° from the normal to the plane of incidence. These data show that the maximum difference in diffraction efficiency does not exceed 0.35% for different incident polarization angles.

Next, we consider the effect of the diffraction grating on the measured signal. While the absolute diffraction efficiency does change as we rotate the polarization of the EUV probe, this change is not of concern for us because our measurements are differential. However, the polarization state of the light reflected from the sample could change due to the magneto-optical rotation. Generally speaking, for the two opposite magnetization directions of the sample $\pm\vec{m}$, the polarization states of the reflected light are different. This could result in different diffraction efficiencies for $+\vec{m}$ and $-\vec{m}$, which would distort the signal. We confirm that this effect is negligible by performing a rigorous coupled wave analysis (RCWA) [58–60] of the grating response to the light reflected from the sample. The results of this analysis are shown in Fig. 9. First, we calculate magneto-optical reflections from the sample using a multilayer approach proposed by Zak *et al.* [57]. Based on the calculated reflections, we determine the polarization state of the reflected light and use it as an input for the RCWA model. We find that, for our conditions, a change in diffraction efficiency for the opposite magnetization directions does not exceed 0.35%, as can be seen from Fig. 9. Such a small change can be safely neglected.

APPENDIX C: ESTIMATION OF THE UNCERTAINTY OF ϵ_{xy}

Because ϵ_{xy} is extracted by use of a fitting procedure based on the multilayer formalism [57] rather than an analytic expression, care must be taken in propagating the errors caused by intensity fluctuations of the EUV probe. This includes several steps. First, we calculate an uncertainty ΔA in the magneto-optical asymmetry defined by Eq. (A4),

$$\Delta A = \sqrt{\left(\frac{\partial A}{\partial R_+}\Delta R_+\right)^2 + \left(\frac{\partial A}{\partial R_-}\Delta R_-\right)^2} = \frac{2\sqrt{R_-^2\Delta R_+^2 + R_+^2\Delta R_-^2}}{(R_+ + R_-)^2}, \tag{C1}$$

where ΔR_+ and ΔR_- are the root-mean-square deviations of the reflected intensities for the positive and negative magnetization directions of the sample, respectively. These quantities were measured at each harmonic peak of the HHG spectrum, and they characterize the stability of the source. In the experiment, the asymmetry was averaged over 100 exposures of the x-ray CCD camera, but only the averaged values were recorded in order to improve the speed of data acquisition. We simulate a normally distributed random set of asymmetries with the calculated standard deviation ΔA and a mean A equal to the measured asymmetry. For each asymmetry from the set, we extract ϵ_{xy} and thus obtain a set of ϵ_{xy} values for which we calculate the root-mean-square deviations at each energy point. This procedure gives us the error bars displayed in Figs. 5 and 8.

APPENDIX D: *AB INITIO* CALCULATION OF ϵ_{xy}

We adopt the same approach for the calculation of ϵ_{xy} as in Ref. [20]. In order to account for the lifetime broadening of the transition from the $3p$ orbital to the conduction band

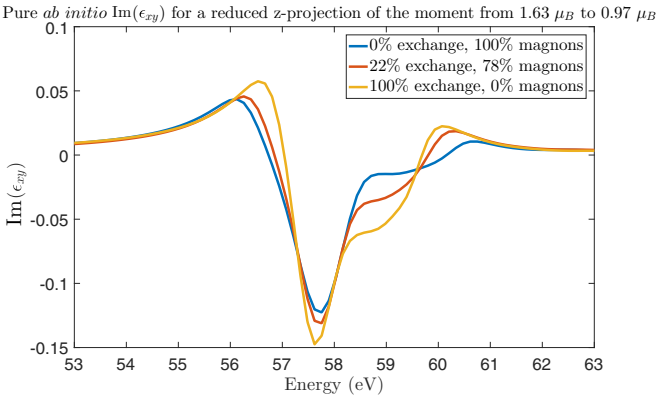

FIG. 10. *Ab initio* calculated ϵ_{xy} of Co without Gaussian broadening and energy shifts for different contributions of the exchange-splitting reduction and magnon excitation. The total demagnetization is 42% for each of the calculated ϵ_{xy} spectra.

and for the exact energy of the $3p$ orbital, we convolve the theoretical ϵ_{xy} with a Gaussian function and apply a small shift in energy, to align the theoretical $3p$-semicore level positions with the measurements. The width and the amplitude of the Gaussian as well as the value of the energy shift are found by a least-square fitting of the ground-state theoretical ϵ_{xy} to the static experimental data. The parameters found from the fit are then applied to the excited-state values of ϵ_{xy} which are compared to the experimental data at 450 fs in Fig. 8. In Fig. 10, we are showing the *ab initio* calculated ϵ_{xy} for various values of exchange splitting and magnon excitation without applying any energy shifts or Gaussian broadening.

All the curves shown in the figure correspond to a reduction of the z-axis projection of the magnetic moment from $1.63\mu_B$ to $0.97\mu_B$, i.e., to 42% demagnetization, and clearly show variations in the spectral shape and energy shifts of the ϵ_{xy} spectrum for reduced values of exchange splitting. This calculation confirms the original prediction made by Erskine and Stern [51].

[1] E. Beaurepaire, J.-C. Merle, A. Daunois, and J.-Y. Bigot, Phys. Rev. Lett. **76**, 4250 (1996).

[2] S. Mangin, M. Gottwald, C.-H. Lambert, D. Steil, V. Uhlíř, L. Pang, M. Hehn, S. Alebrand, M. Cinchetti, G. Malinowski, Y. Fainman, M. Aeschlimann, and E. E. Fullerton, Nat. Mater. **13**, 286 (2014).

[3] S. A. Wolf, D. D. Awschalom, R. A. Buhrman, J. M. Daughton, S. v. Molnár, M. L. Roukes, A. Y. Chtchelkanova, and D. M. Treger, Science **294**, 1488 (2001).

[4] A. V. Chumak, V. I. Vasyuchka, A. A. Serga, and B. Hillebrands, Nat. Phys. **11**, 453 (2015).

[5] B. Koopmans, G. Malinowski, F. Dalla Longa, D. Steiauf, M. Fähnle, T. Roth, M. Cinchetti, and M. Aeschlimann, Nat. Mater. **9**, 259 (2010).

[6] M. Cinchetti, M. Sánchez Albaneda, D. Hoffmann, T. Roth, J.-P. Wüstenberg, M. Krauß, O. Andreyev, H. C. Schneider, M. Bauer, and M. Aeschlimann, Phys. Rev. Lett. **97**, 177201 (2006).

[7] B. Y. Mueller, A. Baral, S. Vollmar, M. Cinchetti, M. Aeschlimann, H. C. Schneider, and B. Rethfeld, Phys. Rev. Lett. **111**, 167204 (2013).

[8] E. Carpene, E. Mancini, C. Dallera, M. Brenna, E. Puppin, and S. De Silvestri, Phys. Rev. B **78**, 174422 (2008).

[9] M. Battiato, K. Carva, and P. M. Oppeneer, Phys. Rev. Lett. **105**, 027203 (2010).

[10] J. Wieczorek, A. Eschenlohr, B. Weidtmann, M. Rösner, N. Bergeard, A. Tarasevitch, T. O. Wehling, and U. Bovensiepen, Phys. Rev. B **92**, 174410 (2015).

[11] G. Malinowski, F. Dalla Longa, J. H. H. Rietjens, P. V. Paluskar, R. Huijink, H. J. M. Swagten, and B. Koopmans, Nat. Phys. **4**, 855 (2008).

[12] A. Melnikov, I. Razdolski, T. O. Wehling, E. T. Papaioannou, V. Roddatis, P. Fumagalli, O. Aktsipetrov, A. I. Lichtenstein, and U. Bovensiepen, Phys. Rev. Lett. **107**, 076601 (2011).

[13] D. Rudolf, C. La-O-Vorakiat, M. Battiato, R. Adam, J. M. Shaw, E. Turgut, P. Maldonado, S. Mathias, P. Grychtol, H. T. Nembach, T. J. Silva, M. Aeschlimann, H. C. Kapteyn, M. M. Murnane, C. M. Schneider, and P. M. Oppeneer, Nat. Commun. **3**, 1037 (2012).

[14] S. Mathias, C. La-O-Vorakiat, P. Grychtol, P. Granitzka, E. Turgut, J. M. Shaw, R. Adam, H. T. Nembach, M. E. Siemens, S. Eich, C. M. Schneider, T. J. Silva, M. Aeschlimann, M. M. Murnane, and H. C. Kapteyn, Proc. Natl. Acad. Sci. U.S.A. **109**, 4792 (2012).

[15] E. Carpene, H. Hedayat, F. Boschini, and C. Dallera, Phys. Rev. B **91**, 174414 (2015).

[16] D. Hinzke, U. Atxitia, K. Carva, P. Nieves, O. Chubykalo-Fesenko, P. M. Oppeneer, and U. Nowak, Phys. Rev. B **92**, 054412 (2015).

[17] A. B. Schmidt, M. Pickel, M. Donath, P. Buczek, A. Ernst, V. P. Zhukov, P. M. Echenique, L. M. Sandratskii, E. V. Chulkov, and M. Weinelt, Phys. Rev. Lett. **105**, 197401 (2010).

[18] A. R. Khorsand, M. Savoini, A. Kirilyuk, A. V. Kimel, A. Tsukamoto, A. Itoh, and T. Rasing, Phys. Rev. Lett. **110**, 107205 (2013).

[19] S. Mathias, C. La-o vorakiat, J. M. Shaw, E. Turgut, P. Grychtol, R. Adam, D. Rudolf, H. T. Nembach, T. J. Silva, M. Aeschlimann, C. M. Schneider, H. C. Kapteyn, and M. M. Murnane, J. Electron Spectrosc. Relat. Phenom. **189**, 164 (2013).

[20] E. Turgut, D. Zusin, D. Legut, K. Carva, R. Knut, J. M. Shaw, C. Chen, Z. Tao, H. T. Nembach, T. J. Silva, S. Mathias, M. Aeschlimann, P. M. Oppeneer, H. C. Kapteyn, M. M. Murnane, and P. Grychtol, Phys. Rev. B **94**, 220408 (2016).

[21] M. F. Tesch, M. C. Gilbert, H.-C. Mertins, D. E. Bürgler, U. Berges, and C. M. Schneider, Appl. Opt. **52**, 4294 (2013).

[22] Z. Q. Qiu and S. D. Bader, J. Magn. Magn. Mater. **200**, 664 (1999).

[23] H.-C. Mertins, S. Valencia, A. Gaupp, W. Gudat, P. M. Oppeneer, and C. M. Schneider, Appl. Phys. A **80**, 1011 (2005).

[24] S. Valencia, A. Gaupp, W. Gudat, H.-C. Mertins, P. M. Oppeneer, D. Abramsohn, and C. M. Schneider, New J. Phys. **8**, 254 (2006).

[25] S. Valencia, A. Kleibert, A. Gaupp, J. Rusz, D. Legut, J. Bansmann, W. Gudat, and P. M. Oppeneer, Phys. Rev. Lett. **104**, 187401 (2010).

[26] J. B. Kortright and S.-K. Kim, Phys. Rev. B **62**, 12216 (2000).

[27] H. Höchst, D. Zhao, and D. L. Huber, Surf. Sci. **352–354**, 998 (1996).

[28] J. Stöhr and H. C. Siegmann, *Magnetism: From Fundamentals to Nanoscale Dynamics* (Springer, Berlin, 2007).
[29] C. T. Chen, Y. U. Idzerda, H.-J. Lin, N. V. Smith, G. Meigs, E. Chaban, G. H. Ho, E. Pellegrin, and F. Sette, Phys. Rev. Lett. **75**, 152 (1995).
[30] A. Weber, F. Pressacco, S. Günther, E. Mancini, P. M. Oppeneer, and C. H. Back, Phys. Rev. B **84**, 132412 (2011).
[31] M. Plötzing, R. Adam, C. Weier, L. Plucinski, S. Eich, S. Emmerich, M. Rollinger, M. Aeschlimann, S. Mathias, and C. M. Schneider, Rev. Sci. Instrum. **87**, 043903 (2016).
[32] S. Eich, M. Plötzing, M. Rollinger, S. Emmerich, R. Adam, C. Chen, H. C. Kapteyn, M. M. Murnane, L. Plucinski, D. Steil, B. Stadtmüller, M. Cinchetti, M. Aeschlimann, C. M. Schneider, and S. Mathias, Sci. Adv. **3**, e1602094 (2017).
[33] M. Hecker, S. Valencia, P. M. Oppeneer, H.-C. Mertins, and C. M. Schneider, Phys. Rev. B **72**, 054437 (2005).
[34] P. M. Oppeneer, H.-C. Mertins, and O. Zaharko, J. Phys.: Condens. Matter **15**, 7803 (2003).
[35] P. M. Oppeneer, in *Handbook of Magnetic Materials*, Vol. 13, edited by K. H. J. Buschow (Elsevier, Amsterdam, 2001), pp. 229–422.
[36] M. Pascolini, S. Bonora, A. Giglia, N. Mahne, S. Nannarone, and L. Poletto, Appl. Opt. **45**, 3253 (2006).
[37] P. B. Corkum, Phys. Rev. Lett. **71**, 1994 (1993).
[38] M. Lewenstein, P. Balcou, M. Y. Ivanov, A. L'Huillier, and P. B. Corkum, Phys. Rev. A **49**, 2117 (1994).
[39] B. L. Henke, E. M. Gullikson, and J. C. Davis, At. Data Nucl. Data Tables **54**, 181 (1993).
[40] L. Guidoni, E. Beaurepaire, and J.-Y. Bigot, Phys. Rev. Lett. **89**, 017401 (2002).
[41] K. Carva, M. Battiato, and P. M. Oppeneer, Phys. Rev. Lett. **107**, 207201 (2011).
[42] M. Fähnle, T. Tsatsoulis, C. Illg, M. Haag, B. Y. Müller, and L. Zhang, J. Supercond. Novel Magn. **30**, 1381 (2017).
[43] C. Illg, M. Haag, and M. Fähnle, Phys. Rev. B **88**, 214404 (2013).
[44] M. Haag, C. Illg, and M. Fähnle, Phys. Rev. B **90**, 014417 (2014).
[45] U. Atxitia, O. Chubykalo-Fesenko, N. Kazantseva, D. Hinzke, U. Nowak, and R. W. Chantrell, Appl. Phys. Lett. **91**, 232507 (2007).
[46] W. Hübner and G. P. Zhang, Phys. Rev. B **58**, R5920 (1998).
[47] A. J. Schellekens and B. Koopmans, Phys. Rev. Lett. **110**, 217204 (2013).
[48] E. C. Stoner, Proc. R. Soc. London, Ser. A **165**, 372 (1938).
[49] C. Herring and C. Kittel, Phys. Rev. **81**, 869 (1951).
[50] M. P. Gokhale and D. L. Mills, Phys. Rev. B **49**, 3880 (1994).
[51] J. L. Erskine and E. A. Stern, Phys. Rev. B **12**, 5016 (1975).
[52] P. M. Oppeneer, J. Sticht, T. Maurer, and J. Kübler, Z. Phys. B **88**, 309 (1992).
[53] M. Stamenova, J. Simoni, and S. Sanvito, Phys. Rev. B **94**, 014423 (2016).
[54] J.-Y. Bigot, M. Vomir, and E. Beaurepaire, Nat. Phys. **5**, 515 (2009).
[55] Z. J. Yang and M. R. Scheinfein, J. Appl. Phys. **74**, 6810 (1993).
[56] C. La-O-Vorakiat, M. Siemens, M. M. Murnane, H. C. Kapteyn, S. Mathias, M. Aeschlimann, P. Grychtol, R. Adam, C. M. Schneider, J. M. Shaw, H. Nembach, and T. J. Silva, Phys. Rev. Lett. **103**, 257402 (2009).
[57] J. Zak, E. R. Moog, C. Liu, and S. D. Bader, Phys. Rev. B **43**, 6423 (1991).
[58] M. G. Moharam and T. K. Gaylord, J. Opt. Soc. Am. **71**, 811 (1981).
[59] M. G. Moharam, T. K. Gaylord, E. B. Grann, and D. A. Pommet, J. Opt. Soc. Am. A **12**, 1068 (1995).
[60] M. G. Moharam, T. K. Gaylord, D. A. Pommet, and E. B. Grann, J. Opt. Soc. Am. A **12**, 1077 (1995).